L-Cysteine-Assisted Tunable Synthesis of PbS of Various Morphologies

ARTICLE *in* THE JOURNAL OF PHYSICAL CHEMISTRY C · OCTOBER 2007

Impact Factor: 4.77 · DOI: 10.1021/jp075096z

L-Cysteine-Assisted Tunable Synthesis of PbS of Various Morphologies

Shenglin Xiong,*,†,‡,§ Baojuan Xi,‡ Dechen Xu,‡ Chengming Wang,§ Xiaoming Feng,§ Hongyang Zhou,‡ and Yitai Qian*,†,‡,§

Department of Materials Science & Engineering, Department of Chemistry, and Hefei National Laboratory for Physical Sciences at Microscale, University of Science and Technology of China, Hefei, Anhui 230026, China

Received: June 29, 2007; In Final Form: August 26, 2007

This article describes a facile L-cysteine-assisted solvothermal method in a mixed solution made of ethylenediamine (en) and distilled water for the large-scale synthesis of various PbS 1D and 3D novel nanostructures. By varying process parameters such as the molar ratio of $Pb(OAc)_2$ to L-cysteine (reactants), the volume ratio of water to ethylenediamine, and the reaction temperature, a variety of 3D architectural structures and a 1D wirelike structure can be controllably synthesized in large quantities. On the basis of early arrested growth (nanowires), a reasonable possible mechanism for the growth of PbS dendritic structures has been proposed. The as-prepared PbS products were examined using diverse techniques including X-ray powder diffraction (XRD), field-emission scanning electron microscopy (FESEM), transmission electron microscopy (TEM), selected-area electron diffraction, high-resolution TEM, Raman spectroscopy, and photoluminescence emission.

1. Introduction

As a member of the important and classical group IV−VI semiconductors, PbS is a well-studied semiconductor with a small band-gap energy (0.41 eV) and a large excitation Bohr radius (18 nm)[1] and is now widely used in many fields, such as infrared (IR) detection, photography, optical switching, and solar absorbtion.[2] Over the past several years, the synthesis of PbS has been extensively explored, and considerable effort has been made to control the size and shape of PbS nanocrystals. At present, a large number of approaches have been reported for the preparation of PbS-based nanostructures, especially dendrite PbS nano- and microstructures. For example, a variety of PbS 1D nanostructures (such as nanowires,[3] nanorods,[4] nanotubes,[5] etc.) have been prepared. Star-shaped PbS nanocrystals were synthesized from the thermal decomposition of a molecular precursor, $Pb(S_2CNEt)_2$.[6] Dendrite PbS was fabricated by a simple hydrothermal process in the presence of surfactant.[7] Hydrothermal/solvothermal routes,[8] a microwave irradiation method,[9a,9b] and an amino-acid-mediated approach[9c] have also been developed to produce PbS nanocrystals with various morphologies.

Although various architectures with nano- and microsize dimensions have been observed for the above-mentioned nanostructures in solution-based processes, the selectively controllable synthesis of various novel PbS nanocrystals has rarely been reported. Therefore, the process of designing and developing new solution-based methods to synthesize novel PbS nanostructures and other similar semiconductors is still a challenging task at present.

Recently, a small biomolecule, L-cysteine, has been introduced to controllably synthesize various metal sulfides in hydrothermal/solvothermal routes.[10] Herein, novel and complex PbS hierarchical structures have been synthesized via an L-cysteine-assisted solvothermal method with use of a mixed solution made of ethylenediamine (en) and distilled water. Furthermore, the shape of the PbS microstructures can be easily modulated from 1D to 3D by controlling the reaction conditions. In this work, we pay more attention to understanding the formation process and growth mechanism of the PbS dendritic nanostructures, as well as some crucial factors that affect hierarchical structures growth. This is a facile method for the selective control of the shape and synthesis of various novel PbS microstructures.

2. Experimental Section

All chemicals were of analytical grade and were directly used without any treatment. In a typical procedure, a given amount of cadmium acetate [$Pb(OAc)_2 \cdot 2H_2O$] and a given amount of L-cysteine ($C_3H_7NO_2S$) were added to a given amount of distilled water, and the mixture was dispersed to form a homogeneous solution by constant strong stirring. Then, a given amount of ethylenediamine (en) was added to the above solution at room temperature; the resulting mixture was continually stirred for 10 min and was then transferred into a Teflon-lined stainless autoclave (60-mL capacity). The autoclave was sealed and maintained at 100−220 °C for 48 h. The system was then cooled to ambient temperature naturally. The final product was collected, washed with distilled water and absolute alcohol several times, vacuum-dried, and kept for further characterization.

The products were characterized by X-ray diffraction (XRD) recorded on a Japanese Rigaku D/max-γA rotating anode X-ray diffractometer equipped with the monochromatic high-intensity Cu Kα radiation ($\lambda = 1.54178$). SEM images were taken with a field-emission scanning electron microscope (FESEM, JEOL-6300F, 15 kV). Microscopy was performed with a Hitachi (Tokyo, Japan) H-800 transmission electron microscope (TEM) at an accelerating voltage of 200 kV, and a JEOL-2010 high-

* To whom correspondence should be addressed. E-mail: xsl8291@ustc.edu.cn (S.X.), ytqian@ustc.edu.cn (Y.Q.). Tel.: 86-551-3607234. Fax: 86-551-3607402.

† Department of Materials Science & Engineering.

‡ Department of Chemistry.

§ Hefei National Laboratory for Physical Sciences at Microscale.

10.1021/jp075096z CCC: $37.00
Published on Web 10/12/2007

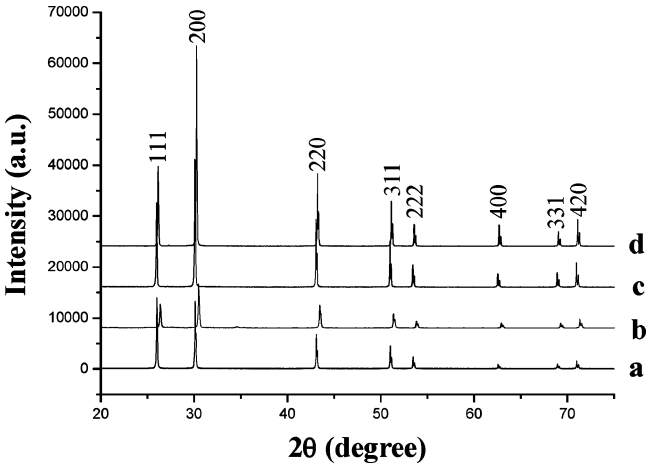

Figure 1. XRD patterns of PbS crystals obtained under different conditions: (a) $Pb(Ac)_2$/L-cysteine = 1:2, 220 °C for 48 h; (b) $Pb(Ac)_2$/L-cysteine = 2:1, 220 °C for 48 h; (c) $Pb(Ac)_2$/L-cysteine = 2:1, 150 °C for 48 h; and (d) $Pb(Ac)_2$/L-cysteine = 3:1, 150 °C for 48 h. V_{water}/V_{en} = 2:3.

resolution TEM, also at 200 kV. Raman spectra were recorded on a Jobin Yvon (Villeneuve d'Ascq, France) LABRAM-HR confocal laser micro-Raman spectrometer at room temperature. Photoluminescence (PL) measurements were carried out with a Perkin-Elmer LS-55 luminescence spectrometer using a pulsed Xe lamp.

3. Results and Discussion

3.1. Selective Synthesis of Various PbS Hierarchical Structures: Influence of the Volume Ratio of Mixed Solvents. In our experiments, by varying the experimental conditions such as the reagent ratios, the volume ratio of ethylenediamine and water, and the reaction temperature, PbS nanocrystals with controllable morphologies were conveniently obtained using our proposed method.

Figure 1 shows the X-ray diffraction (XRD) patterns of the as-prepared products at different water/en volume ratios with the same initial reactant concentrations. The diffraction patterns distinctly indicate the fine crystallinity of the obtained samples. The reflection peaks of the different products can be indexed as face-centered cubic (fcc) rock-salt-structured PbS with a lattice constant of a = 5.926 Å, which is in good agreement with the literature values (JCPDS Card No. 05-592, a = 5.936 Å). No peaks of impurities were detected, revealing the high purity of the as-synthesized products.

The morphology and microstructure of the resulting products were investigated using field-emission scanning electron microscopy (FESEM). Figure 2demonstrates that various PbS nanostructures were prepared by varying the reaction media. Figure 2a exhibits the general morphology of the product in a binary solution with a V_{water}/V_{en} volume ratio of 3:2. A higher-magnification SEM image (Figure 2b) shows a typical PbS microcrystal with a hierarchical nanostructure, from which one can clearly see that the PbS hierarchical structure is constructed from a stem (the primary structure) with four nanorod limbs (the secondary structure) that epitaxially grew on this stem and are perpendicular to both the stem and each other. Figure 2c indicates a more complex 3D hierarchical structure in which, in addition to the primary and secondary structures, nanorod limbs (the tertiary structure and quaternary structure) epitaxially grew on those secondary and tertiary nanorods, respectively, perpendicular to each other. Among the structures, the primary structures are the longest, and the quartus structures are the shortest.

When the V_{water}/V_{en} volume ratio was decreased to 2:3, propeller arraylike structures were obtained (Figure 2d−f). Figure 2d shows a view of the well-aligned PbS propeller arrays with typical lengths in the range of 10−30 μm. High-magnification FESEM images (Figure 3e,f) reveal that each prism of propeller arrays consists of four arrays of tetragonal nanoblades that are 2−5 μm in length. Prisms of the propellers remain their fourfold array of nanorod blades around the central nanorod, and all of these blades have a uniform tetragonal shape. These blades were perpendicular to the central nanorods and perpendicular to each other. To the best of our knowledge, the synthesis of such novel PbS 3D hierarchical structures has never previously been reported.

Interestingly, when the V_{water}/V_{en} volume ratio was continually decreased to 1:4, as shown in Figure 2g, the resulting product was composed of flowerlike structures. Figure 2h is a high-magnification TEM image, representing the typical flower shape of four petals. To observe the substructure of the petal, a higher-magnification TEM image is shown in Figure 2i. It is clear that the tip tapers off and cubes with an angle truncated in an orderly fashion that is self-assembled along the stalk.

The morphology and structure of the PbS nanopropeller arrays were further confirmed by TEM and selected-area electron diffraction (SAED). Figure 3a shows a typical TEM image of an individual PbS nanopropeller array. The single-crystalline nature of the PbS propellers was further revealed by selected-area electron diffraction (SAED). SAED patterns recorded from the left branch, the trunk, and the right branch in a single propeller are displayed in Figure 3b−d, revealing that the SAED patterns are almost the same and were all recorded along the $[01\bar{1}]$ zone axis of the cubic phase of PbS. These patterns further confirm the single crystallinity of the as-prepared products.

3.2. Influence of the Pb^{2+}-to-L-Cysteine Molar Ratio. In our experiments, it was found that the variation of the precursor-to-L-cysteine molar ratio afforded a very facile way to control the morphology of the PbS nanocrystals. Then, we considered the products at the volume ratio of V_{water}/V_{en} = 2:3 for an example to illustrate the problem. When the Pb^{2+}-to-L-cysteine molar ratio was increased to 3:1, with reaction for 48 h at 220 °C (see Figure 4a), the products mainly consisted of candlelike submicrorods with stem and tip diameters in the ranges of 500−700 and 200−300 nm, respectively, obviously different from the morphology of the above-mentioned products in Figure 2d−f. TEM images further confirm the candlelike structures. Figure 4b indicates a typical low-magnification TEM image of a single PbS candlelike submicrorod with a stem diameter of about 700 nm and a tip diameter of about 300 nm. In the HRTEM image of Figure 4c recorded from Figure 4b, the fringe spacing of 0.30 nm observed in this image is close to the (200) lattice plane of PbS, revealing that the candlelike submicrorod is single-crystalline in nature and grows preferentially along the [100] direction. The growth pattern is consistent with the results reported in refs 3b, 4, and 7.

Surprisingly, when the Pb^{2+}-to-L-cysteine molar ratio was decreased to 1:2, with reaction for 48 h at 220 °C (see Figure 5), the products mainly consisted of hollow cubic structures with edge lengths ranging from 3 to 8 μm, and with the proportion of hollow cubes in the sample estimated to be above 50%. A panoramic image of the sample is shown in Figure 5a, from which some interesting phenomena can be observed: On one hand, some cubes in the samples have a layered concavity on each of their faces (Figure 5b). On the other hand, some small

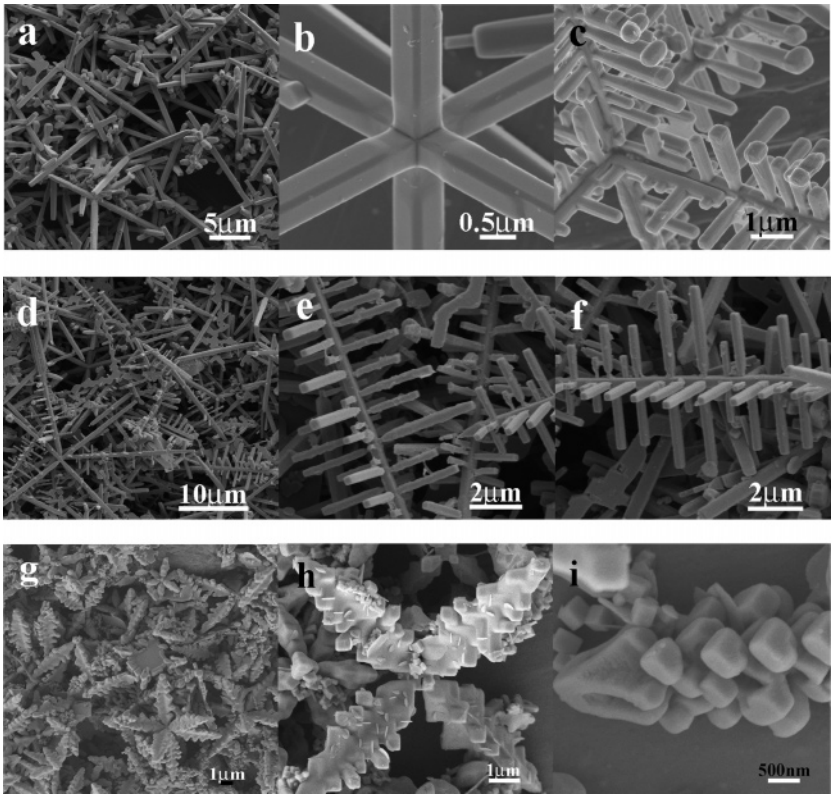

Figure 2. FESEM images of the products prepared at various volume ratios of mixed solvents (V_{water}/V_{en}): (a−c) 3:2, (d−f) 2:3, and (g−i) 1:4. Pb^{2+}/L-cysteine = 2:1, with reaction for 48 h at 220 °C.

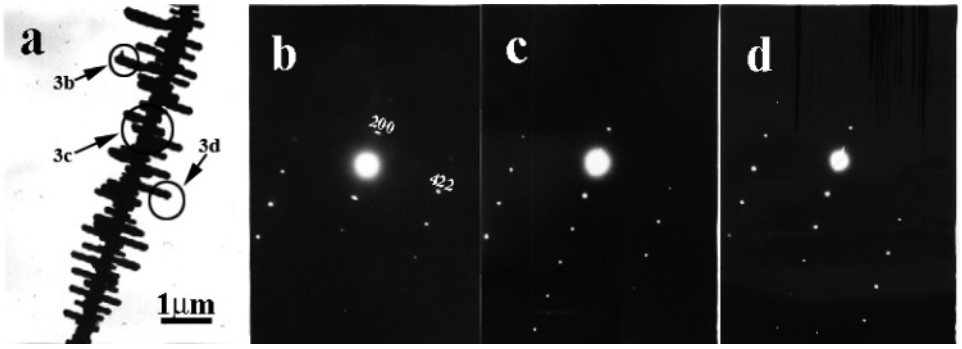

Figure 3. (a) TEM image of an individual PbS propeller array and (b−d) SAED patterns taken from the left branch, the trunk, and the right branch in a single propeller array, as marked in Figure 3a.

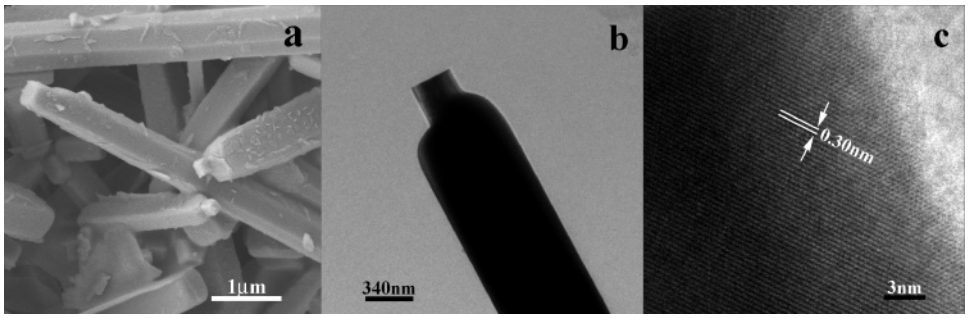

Figure 4. (a,b) FESEM and (c,d) TEM (HRTEM) images of the products prepared at Pb^{2+}/L-cysteine = 3:1, V_{water}/V_{en}=2:3, with reaction for 48 h at 220 °C.

cubes assemble with each other into a central hollow superstructure. Figure 5c,d clearly reveals that the superstructure is constructed from the assembly of eight cubes, with every four small cubes in the same plane.

3.3. Influence of Reaction Temperature. To investigate the influence of temperature on the morphology, we again considered the products at the volume ratio of V_{water}/V_{en} = 2:3 as an example. It was found that temperature significantly affected the shape of the particles. When the temperature was decreased to 150 °C, the shape of products was obviously different from that observed at 220 °C (Figure 2d−f). Figure 6a shows a typical low-magnification SEM image of the products prepared at the molar ratio of Pb^{2+}/L-cysteine = 2:1, which demonstrates the PbS nanostructures consist of a uniform dendritic structure. From

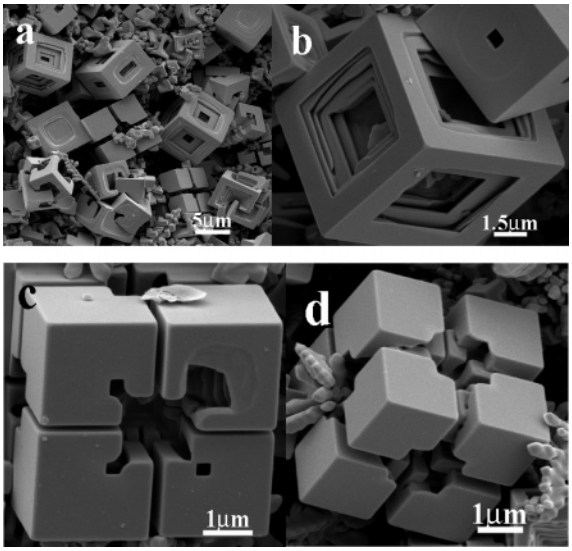

Figure 5. FESEM images of the PbS boxes: (a) panoramic image and (b) magnified image. The products were fabricated at 220 °C for 48 h in mixed solution with V_{water}/V_{en} = 2:3 and Pb^{2+}/L-cysteine = 1:2.

the high-magnification SEM image (Figure 6b), one can clearly observe that each individual PbS dendrite has 3D structures with one long central trunk (the length of which is in the range of 10−20 μm) and four short lateral branches. The nanorods in each branch arrange in the same plane, parallel to each other and perpendicular to the central trunk. Detailed observation further demonstrates that the branches (nanorods) are in a prism shape with a tetragonal cross section (Figure 6c). Interestingly, when the Pb^{2+}/L-cysteine molar ratio was increased to 3:1, the morphology of the products showed a subtle change (see Figure 6d−f). From the low-magnification SEM image (Figure 6d), one can see the product still is made up of a well-defined dendritic structure. However, careful observation distinctly reveals that the branches are in a backbone shape with a tapered cross section. To the best of our knowledge, the synthesis of such novel PbS 3D hierarchical structures has never previously been reported. Meanwhile, our results also further demonstrate that the molar ratio of the reagents has a significant effect on the morphology of the product.

3.4. Time-Dependent Experiments. To study the growth mechanism of various PbS structures, we considered the dendritic structures as an example and performed a series of experiments for different lengths of time, as discussed below. We followed the nucleation and growth steps taken at various stages of reaction by TEM and XRD. An offwhite suspension was observed to form after the mixture solution had been aged at 150 °C for 30 min. Figure 7a shows a TEM image of the product obtained at this stage, which reveals the product consisted of wirelike nanostructures with diameters of 50−200 nm and length up to tens of micrometers. These nanowires were characterized by XRD, which suggested that they were well crystallized (Figure 8a). The inset electron diffraction (ED) pattern in Figure 7a demonstrates the polycrystallinity of these nanowires. Both XRD and ED results are consistent with what had previously been reported.[11] The likely chemical structure of the initial nanowires is $HSCH_2CH(NH_2)COO-Pb-OH$, which means that $HSCH_2CH(NH_2)COO-Pb-OH$, and not PbS, formed first. Meanwhile, FTIR analyses also demonstrate that the likely chemical structure of the precursor nanowires is $HSCH_2CH(NH_2)COO-Pb-OH$ by comparison to the IR spectrum of pure cysteine (see Supporting Information, Figure S1). In the environment of a weakly basic solvent, such as ethanolamine, which supplies OH^- ions, the proton of the COOH group is removed, and the Pb^{2+} ions could react with cysteine to form the precursor nanowires. Direct evidence for the hypothesis requires further study, and this work is under way. When the reaction time was increased to 60 min, the morphology of the products changed markedly. As shown in Figure 7b, a minority of dendritic structures and nanowires coexisted in the products. SAED patterns recorded from the nanowire and dendritic structures, as marked in Figure 3b, can be indexed to a polycrystalline $HSCH_2CH(NH_2)COO-Pb-OH$ phase and single crystalline PbS, respectively. Increasing the aging time resulted in the formation of more dendritic structures. As the aging time increased, it was clearly observed that the dendritic structures gradually increased in the quantity and, at the same time, the nanowires gradually reduced and completely disappeared after 4 h, as shown in Figure 7c,d, respectively. That is, the PbS nanostructures grew at the expense of the precursor nanowires, which can also be understood by contrasting the variations in the peak intensity in the XRD patterns of the products prepared at 30, 60, 120, and 240 min (shown in Figure 8). The characteristic peaks of PbS were markedly intensified, and those of precursor were weakened and finally disappeared when the reaction time was extended to 4 h.

When another sulfur source (for instance, thioacetamide and thiourea) replaced L-cysteine, no polycrystalline $HSCH_2CH(NH_2)COO-Pb-OH$ nanowires formed in the initial reaction stage, and no dendritic structures were obtained in the final products (see Figure 9). To determine whether the formation of incipient polycrystalline nanowires is a key step in the development of the dendritic structure, we used polycrystalline $HSCH_2CH(NH_2)COO-Pb-OH$ nanowires, obtained by collecting the deposit on the bottom of autoclave, as the starting material. It was found that a large number of dendritic structures were formed. These experiments confirmed that the initially formed precursor [polycrystalline $HSCH_2CH(NH_2)COO-Pb-OH$ nanowires] is a crucial component in the formation of the PbS dendritic nanostructures.

The present procedure for the formation of various PbS hierarchical structures differs from other reaction systems in that a precursor is involved. In the initial stage, L-cysteine reacts with Pb^{2+} and hydroxyl ion (OH^-) to form polycrystalline $HSCH_2CH(NH_2)COO-Pb-OH$ nanowires. These nanowires were not stable under the given reaction conditions and had a tendency to decompose into PbS. That is, $HSCH_2CH(NH_2)COO-Pb-OH$ served as the real precursor to PbS. Therefore, the formation procedure of the PbS nanostructures can be formulated as follows:

$$Pb^{2+} + \text{L-cysteine} + OH^- \rightarrow HSCH_2CH(NH_2)COO-Pb-OH \quad (1)$$

$$HSCH_2CH(NH_2)COO-Pb-OH \rightarrow PbS \quad (2)$$

In most reported colloidal syntheses of metal or semiconductor 1D nanocrystals, the anisotropic growth of the 1D structure is often driven by using capping ligands that can bind selectively onto particular facets of the seed particles.[12] Therefore, it is reasonable to conclude that, in our approach, the reagent ethylenediamine might adsorb onto the special faces of the incipient PbS nuclei. The selective absorption of ethylenediamine onto some facets not only prevents the particles from agglomeration but also influences the growth of these planes, which strongly favors anisotropic growth of the PbS nuclei along

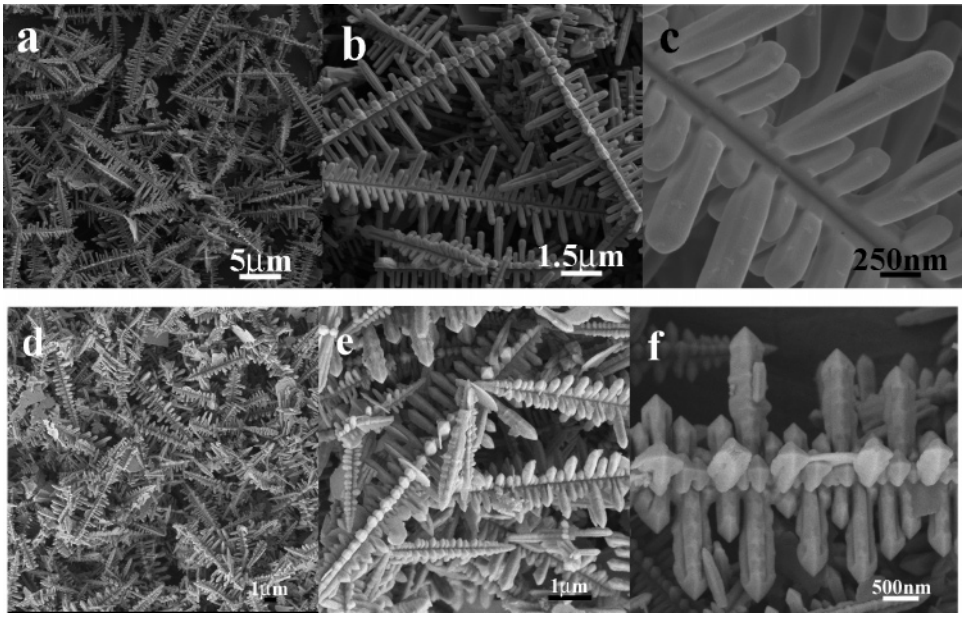

Figure 6. FESEM images of the products prepared at various precursor-to-L-cysteine molar ratios (Pb^{2+}/L-cysteine): (a−c) 2:1 and (d−f) 3:1. V_{water}/V_{en}= 2:3, with reaction for 48 h at 150 °C.

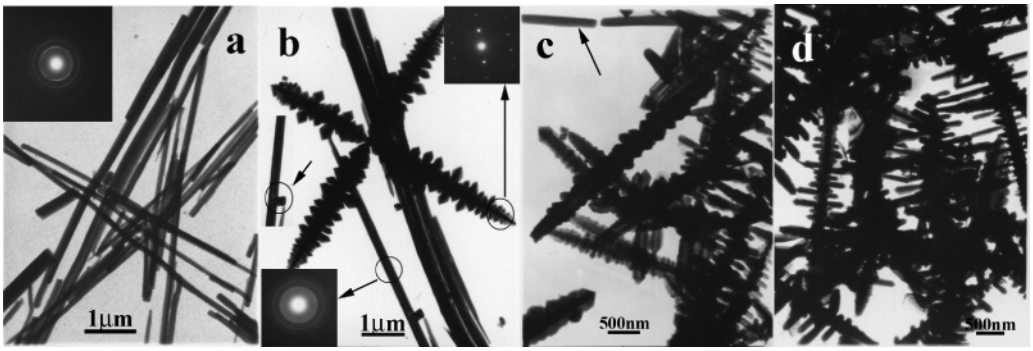

Figure 7. Typical TEM images of samples during the formation of PbS nanosphere self-assembled nanorods recorded at different times: (a) 0.5, (b) 1, (c) 2, and (d) 4 h.

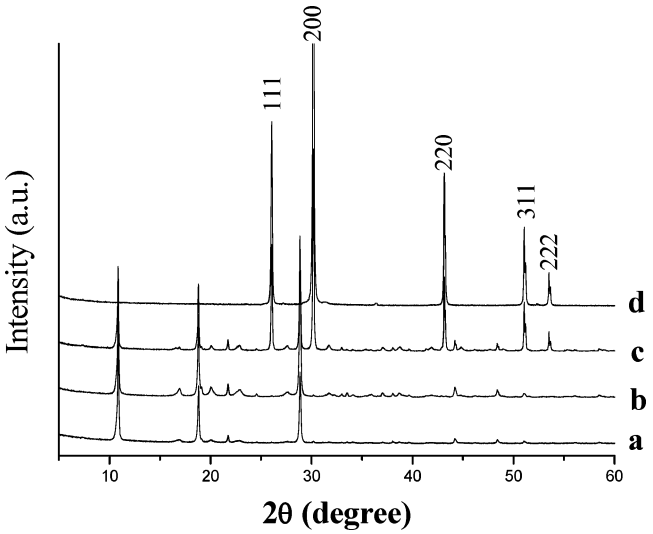

Figure 8. XRD patterns of samples during the formation of PbS dendritic structure obtained at different growth stages: (a) 0.5, (b) 1, (c) 2, and (d) 4 h.

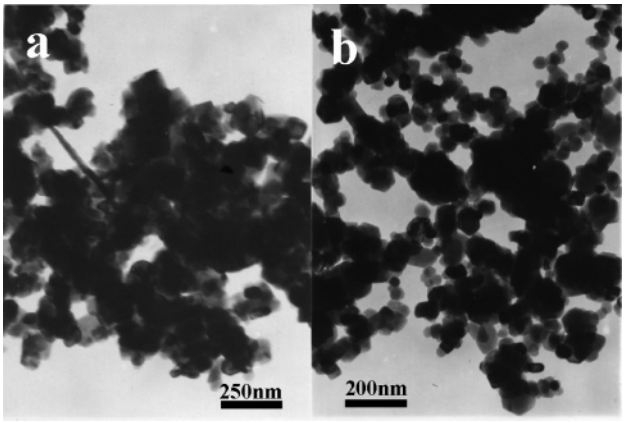

Figure 9. TEM images of samples prepared under similar conditions but with L-cysteine replaced by (a) thioacetamide [$Pb(OAc)_2$/thioacetamide = 2:1] and (b) thiourea [$Pb(OAc)_2$/thiourea = 2:1]. The products were fabricated at 150 °C for 48 h in mixed solutions with V_{water}/V_{en}= 2:3.

the [100] axis, as further confirmed by the HRTEM results. In the synthesis of inorganic nanostructures, this might accord with the fact that crystal growth is modulated extrinsically by solvent absorption on certain crystallographic facets, which inhibits the growth of some crystal planes and leads to different growth rates during the growth process of the particles, thus generating certain novel crystal shapes.[13] As reported previously,[14] ethylenediamine acts as a structure-directing coordination molecular template (SCMT) responsible for the morphologies of the resulting products. In our experiments, ethylenediamine rightly

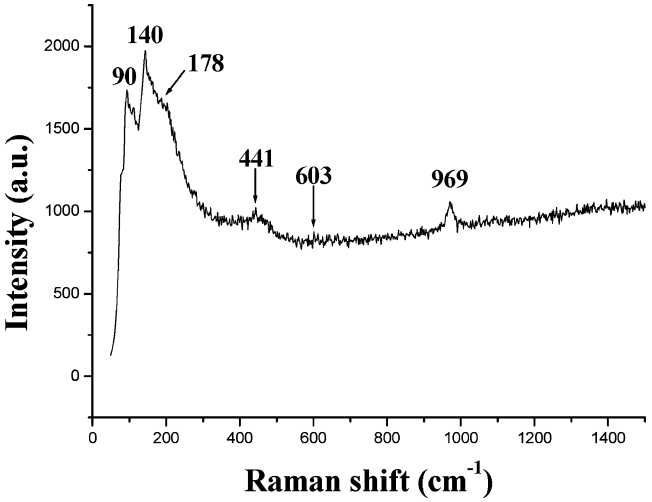

Figure 10. Room-temperature Raman spectrum of PbS dendritic structures.

played the role of directing the structure growth, generating a variety of novel PbS nanostructures, as can be further confirmed by the experimental result that only PbS nanoparticles could be obtained in the product with pure water as the solvent.

On the basis of the above results and analyses, the formation of precursor $HSCH_2CH(NH_2)COO-Pb-OH$ nanowires can be regarded as a crucial step for the formation of PbS nanostructures. The whole process is a special in situ decomposition of the precursor polycrystalline nanowires providing PbS units that served as the seeds for the subsequent nucleation and growth of PbS nanostructures. From the inset of Figure 7b, it is clearly observed that PbS preferentially grew in the longitudinal direction, the ⟨100⟩ direction, to form the long trunk and then grew along the ⟨011⟩ direction to form the branches originating from the above-mentioned structure-directing role of ethylenediamine. The L-cysteine-assisted binary solution system is quite complicated, and the formation of certain nanostructure needs further development. Obviously, the synergetic effects of ethylenediamine (en) and water could also exert a key influence on the morphology of the PbS nanostructures. Further work to better understand the formation of certain PbS nanostructures is still under way.

The Raman spectrum of the as-prepared PbS dendritic structures (Figure 10) indicates six bands in the range of 50−1200 cm^{-1}, located at around 90, 140, 178, 441, 603, and 969 cm^{-1}. The peak at ∼90 cm^{-1} resembles the peak at ∼68 cm^{-1} recorded at 4.3 K with 584 nm as the excitation length and is an acoustic mode.[15] Similarly to the ∼150 cm^{-1} peak[15a] recorded at 4.3 K with excitation at 584 nm and the 155 cm^{-1} peak[16a] recorded with 632.8-nm excitation, the strong band centered at 140 cm^{-1} also originates from the combination of longitudinal and transverse acoustic modes.[16b] Additionally, a weak band at about 178 cm^{-1} usually comes from the fundamental longitudinal optical (LO) phonon mode,[15,16b] and those at 441 and 603 cm^{-1} are from its first and second overtones (2LO and 3LO), respectively.[15b,16b] It has been reported that the band centered at 961 cm^{-1} could arise from sulfates in the sample not the laser-induced degradation.[16b] However, in our sample, the XRD pattern of the PbS dendritic structures confirms that the product consists of pure cubic PbS without the presence of sulfates. As a result, the band centered at 961 cm^{-1} could be due to sulfates in the sample originating from the laser-induced degradation, which is consistent with results reported previously.[8d] The Raman spectra of the other PbS novel nanostructures are similar to that of PbS dendritic structures.

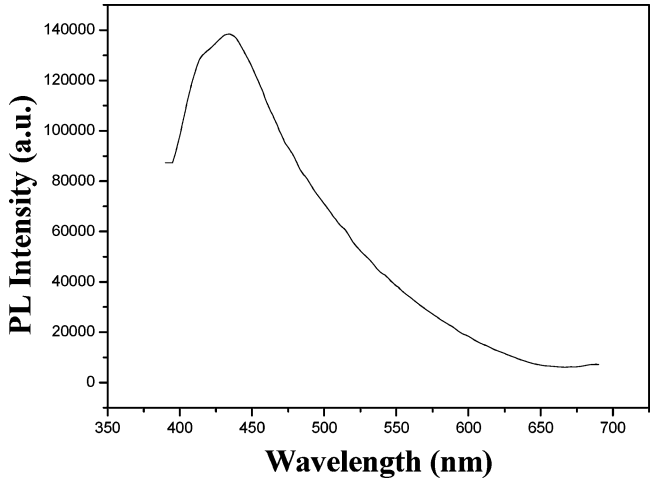

Figure 11. Room-temperatsure photoluminescence spectrum of PbS dendritic structures.

Figure 11 shows a typical PL spectrum (λ_{exc} = 360 nm) of PbS dendritic structures that was measured using a Perkin-Elmer LS-55 luminescence spectrometer with an excitation slit width of 5 nm and an emission slit width of 5 nm. A sharp and strong peak centered at a wavelength of 433 nm is observed. Emission bands at 433 nm are usually related to the transition of electrons from the conduction band edge to holes, trapped at interstitial Pb^{2+} sites. As reported previously,[17] the emission at about 433 nm presents a Stokes shift compared to the absorption band edge (246 nm) in the UV−vis absorption spectra. The detail of the electron-transport mechanism for PbS dendritic structures is worthy of further study.

4. Conclusions

In conclusion, a simple procedure based on an L-cysteine-assisted method has been developed to selectively and controllably synthesize PbS nanocrystals with 1D structures and novel 3D superstructures in high yield in a binary solution by controlling the reaction conditions, such as the molar ratio between $Pb(OAc)_2$ and L-cysteine and the volume ratio of the mixed solvents. The formation mechanism of the dentritic structures was investigated in detail through TEM observations. The PL emission at about 433 nm can be attributed to transitions between states in excitons that are trapped on nanocrystal surfaces. It is reasonable to expect that this simple approach can easily be scaled up to prepare various PbS nano-/microstructures for important applications in the large field of nanotechnologies.

Acknowledgment. The financial support of this work by the China Postdoctoral Science Foundation, the National Natural Science Foundation of China (Grant 20431020), and the 973 Project of China (Grant 2005CB623601), is gratefully acknowledged.

Supporting Information Available: FTIR spectra of the precursor nanowires and pure cysteine. This material is available free of charge via the Internet at http://pubs.acs.org.

References and Notes

(1) Machol, J. L.; Wise, F. M.; Patel, R. C.; Tanner, D. B. *Phys. Rev. B* **1993**, *48*, 2819.

(2) (a) Orletskii, V. B.; Teterkin, V. V.; Sizov, F. F.; Gutsulyak, V. G.; Tashtawbaev, N. O. *Ukr. Fiz. Zh. (Russ. Ed.)* **1994**, *39*, 505. (b) Kondas, P. A. *Report ARFSD-TD-92024*; Government Reports and Announcements Index; U.S. Government Printing Office: Washington, DC, 1993. (c)

Harman, T. C. PCT International Patent Application WO 9416465, 1994 (U.S. Patent Application 2,451,121, 1993).

(3) (a) Gao, F.; Yang, P.; Liu, X.; Zhao, D. *Nano Lett.* **2001**, *1*, 743. (b) Yu, D. B.; Wang, D. B.; Meng, Z. Y.; Lu, J.; Qian, Y. T. *J. Mater. Chem*. **2002**, *12*, 403. (c) Ge, J. P.; Wang, J.; Zhang, H. X.; Wang, M. X.; Peng, Q.; Li, Y. D. *Chem. Eur. J.* **2005**, *11*, 1889.

(4) Wang, S.; Yang, S. *Langmuir* **2000**, *16*, 389.

(5) Patzke, G. R.; Krumeich, F.; Nesper, R. *Angew. Chem., Int. Ed.* **2002**, *41*, 2446.

(6) Lee, S. M.; Jun, Y. W.; Cho, S. N.; Cheon, J. W. *J. Am. Chem. Soc.* **2002**, *124*, 11244.

(7) Kuang, D. B.; Xu, A. W.; Fang, Y. P.; Liu, H. Q.; Frommen, C.; Fenske, D. *Adv. Mater.* **2003**, *15*, 1747.

(8) (a) Zhou, G. J.; Lu, M. K.; Xiu, Z. L.; Wang, S. F.; Zhang, H. P.; Zhou, Y. Y.; Wang, S. M. *J. Phys. Chem. B* **2006**, *110*, 6543. (b) Zhao, P. T.; Wang, J. M.; Cheng, G.; Huang, K. X. *J. Phys. Chem. B* **2006**, *11*, 22400. (c) Ma, Y. R.; Qi, L. M.; Ma, J. M.; Cheng, H. M. *Cryst. Growth Des*. **2004**, *4*, 351. (d) Cao, H. Q.; Wang, G. Z.; Zhang, S. C.; Zhang, X. R. *Nanotechnology* **2006**, *17*, 3280. (e) Zhang, W. Q.; Yang, Q.; Xu, L. Q.; Yu, W. C.; Qian, Y. T. *Mater. Lett.* **2005**, *59*, 3383. (f) Wang, D. B.; Yu, D. B.; Shao, M. W.; Liu, X. M.; Yu, W. C.; Qian, Y. T. *J. Cryst. Growth* **2003**, *257*, 384. (g) Xu, L. Q.; Zhang, W. Q.; Ding, Y. W.; Yu, W. C.; Xing, J. Y.; Li, F. Q.; Qian, Y. T. *J. Cryst. Growth* **2004**, *273*, 213.

(9) (a) Ni, Y. H.; Liu, H. J.; Wang, F.; Liang, Y. Y.; Hong, J. M.; Ma, X.; Xu, Z. *Cryst. Growth Des.* **2004**, *4*, 759. (b) Cao, H. L.; Gong, Q.; Qain, X. F.; Wang, H. L. Zai, J. T.; Zhu, Z. K. *Cryst. Growth Des*. **2007**, *7*, 425. (c) Lu, Q. Y.; Gao, F.; Komarmeni, S. *Nanotechnology* **2006**, *17*, 2574.

(10) (a) Chen, X. Y.; Zhang, X. F.; Shi, C. W.; Li, X. L.; Qian, Y. T. *Solid State Commun.* **2005**, *134*, 613. (b) Chen, X. Y.; Zhang, X. F.; Wang, Z. H.; Wan, J. X.; Qain, Y. T. *Mater. Chem. Phys.* **2006**, *98*, 419. (c) Chory, C. B.; Remenyi, C.; Strohm, H.; Müller, G. *J. Phys. Chem. B* **2004**, *108*, 7637. (d) Zhang, B.; Ye, X. C.; Dai, W.; Hou, W. Y.; Xie, Y. *Chem. Eur. J.* **2006**, *12*, 2337. (e) Zhang, B.; Ye, X. C.; Hou, W. Y.; Xie, Y. *J. Phys. Chem. B* **2006**, *98*, 419. (f) Xiong, S. L.; Xi, B. J.; Wang, C. M.; Zou, G. F.; Fei, L. F.; Wang, W. Z.; Qain, Y. T. *Chem. Eur. J.* **2007**, *13*, 3076. (g) Xiong, S. L.; Xi, B. J.; Wang, C. M.; Xu, D. C.; Feng, X. M.; Zhu, Z. C.; Qian, Y. T. *Adv. Funct. Mater*., available as an Early View article (DOI: 10.1002/adfm.200600891).

(11) Tong, H.; Zhu, Y. J.; Yang, L. X.; Li, L.; Zhang, L. *Angew. Chem., Int. Ed.* **2006**, *45*, 7739.

(12) (a) Peng, X. G.; Manna, L.; Yang, W. D.; Wickham, J.; Scher, E.; Kadavanich, A.; Alivisatos, A. P. *Nature* **2000**, *404*, 59. (b) Cordente, N.; Respaud, M.; Senocq, F.; Casanove, M. J.; Amiens, C.; Chaudret, B. *Nano Lett.* **2001**, *1*, 565. (c) Jun, Y. W.; Lee, S. M.; Kang, N. J.; Cheon, J. *J. Am. Chem. Soc.* **2001**, *123*, 5150.

(13) (a) Johnson, C. J.; Dujardin, E.; Davis, S. A.; Murphy, C. J.; Mann, S. *J. Mater. Chem*. **2002**, *12*, 1765. (b) Yu, S. H.; Cölfen, H.; Tauer, K.; Antonietti, M. *Nat. Mater*. **2004**, *4*, 51. (c) Wang, L.; Chen, X.; Zhan, J.; Sui, X.; Xhao, J.; Sun, Z. *Chem. Lett*. **2004**, 720. (d) Murphy, C. J. *Science* **2002**, *298*, 2139.

(14) Peng, Q.; Dong, Y. J.; Deng, Z. X.; Sun, X. M.; Li, Y. D. *Inorg. Chem*. **2001**, *40*, 3840.

(15) (a) Krauss, T. D.; Wise, F. W. *Phys. Rev. B* **1997**, *55*, 9860. (b) Krauss, T. D.; Wise, F. W.; Tanner, D. B. *Phys. Rev. Lett.* **1996**, *76*, 1376. (c) Krauss, T. D.; Wise, F. W. *Phys. Rev. Lett.* **1997**, *79*, 5102.

(16) (a) Sherwin, R.; Clark, R. J. H.; Lauck, R.; Cardona, M. *Solid State Commun.* **2005**, *134*, 565. (b) Smith, G. D.; Firth, S.; Clark, R. J. H.; Cardona, M. *J. Appl. Phys.* **2002**, *92*, 4375.

(17) Fan, M. G., Ed. *Fundamental of Photochemistry and Photonics Materials Science*; Science Press: Beijing, 2001.